The Effect of Temperature Gradients on Stress Development during Cryopreservation via Vitrification

PAUL S. STEIF, MATTHEW C. PALASTRO, and YOED RABIN

ABSTRACT

This study addresses the problem of thermal stress development in bulky specimens during cryopreservation via vitrification (vitreous means glassy in Latin). While this study is a part of an ongoing effort to associate the developing mechanical stress with the relevant physical properties of the cryopreserved media and to its the thermal history, the current paper focuses exclusively on the role of temperature gradients. Temperature gradients arise due to the high cooling rates necessary to facilitate vitrification; the resulting nonuniform temperature distribution leads to differential thermal strain, possibly resulting in cracking. The cooling rate is assumed constant on the outer surface in this study, and the material properties are assumed constant. It is demonstrated that under these assumptions, mechanical stress develops only when the temperature distribution in the specimen approaches thermal equilibrium at a cryogenic storage temperature. It is shown that the maximum possible stresses for a given cooling rate can be computed with a simple thermoelastic analysis; these stresses are associated with cooling to sufficiently low temperatures, and are independent of the variation of viscosity with temperature. Analytic estimates for these stresses are obtained for several idealized shapes, while finite element analysis is used to determine stresses for geometries used in cryopreservation practice. Stresses that develop under a wider range of storage temperatures are also studied with finite element analysis, and the results are summarized with suitable normalizations. It is found that no stresses arise if cooling ceases above the set temperature, which defines the transition from viscous-dominated to elastic-dominated behavior; the set temperature is determined principally by the dependency of viscosity upon temperature. Strategies for rapidly reaching low temperatures and avoiding high stresses are inferred from the results.

INTRODUCTION

SINCE THE ADVENT of transplantation science, cryopreservation has been recognized as a highly desirable method for facilitating availability of the highest quality material. This goal has been achieved in some cellular systems, but extrapolation to organized tissues and organs is fraught with additional problems that have only recently been addressed. Application of the principles of cryobiology to the growing needs of the emerging tissue engineering field, for example, tissue-engineered blood vessels, has emphasized the need for greater understanding of the fundamentals of low-temperature preservation as they apply to three-dimensional multicellular tissues. In particular, an understanding of the thermomechanical stresses that arise during cryopreservation of complex biological systems, and their tendency to cause fracture, is crucial for the development of improved methods of storage. This important aspect of cryobiology has thus far received little attention, whereas the basic tools necessary for the study of these fundamental problems have not been available.

Most theoretical studies of the development of mechanical stress during cryopreservation have presumed an elastic response in the tissue.[1–5] This assumption could be justified in the

Biothermal Technology Laboratory, Department of Mechanical Engineering, Carnegie Mellon University, Pittsburgh, Pennsylvania.

case of tissue crystallization, which is not typical in cryopreservation. In the case of a tissue permeated with a cryoprotective agent (CPA) and cooled at a sufficiently high rate, crystallization can potentially be avoided; instead, the material transitions to glass as it undergoes a steady but dramatic increase in viscosity. Glass transition in the context of cryopreservation is typically referred to as vitrification, where "vitreous" in Latin means glass. However, pure vitrification can only be associated with pure CPAs, while in the tissue–CPA system partial vitrification is expected, and the quality of vitrification is the subject matter of many cryobiology studies.[6–8] Analysis of mechanical stress during vitrification has been paid very little attention over the years, and only recent studies have begun to address modeling and worst case scenarios of mechanical stress during cryopreservation via vitrification.[9–12] The resulting mechanical stresses during vitrification can potentially exceed the strength of the material, leading to its fracturing, which is a significant barrier to the cryopreservation of three-dimensional multicellular tissues.

While the quality of cryopreservation is dependent on the level of mechanical stress developed in the tissue, vitrification as an alternative to cryopreservation has several potential advantages from the biological standpoint.[6,7,13,14] Here, ice crystallization can be avoided, which is known to be the cornerstone of cryoinjury. No appreciable degradation occurs over time in living matter trapped within a vitreous matrix, and vitrification is potentially applicable to all biological systems. However, vitrification is associated with a high CPA concentration, which is potentially very toxic, and CPA cocktails are currently studied by various research groups to overcome this obstacle. Other difficulties with vitrification are known to be associated with uniform permeation of the tissue with the CPA.

The current study represents another step in an ongoing effort to develop tools to quantify mechanical stress and the propensity for fracture during vitrification. Previous work focused on the consequences of constraining the thermal contraction of the vitrifying specimen; theoretical and experimental studies of a CPA droplet vitrifying on a substrate gave insight into the role of viscosity and the level of strain at which vitrified CPA may crack.[12] The constraining effect of vial walls on the thermal contraction of the contained CPA medium was later studied and used to rationalize crack propagation patterns in the CPA.[10] Also recently, the potential effect of partial vitrification and partial crystallization on cracking was investigated,[11] including its dependency on various mechanical properties of the CPA. The current study sets aside effects of constraint and inhomogeneity in properties and addresses exclusively the effect of temperature gradients on stress and cracking in a homogeneous region of CPA. Significant temperature gradients arise when a specimen of a significant size is cooled from outside in and become increasingly severe as the cooling rate increases.

The current report starts with a presentation of the material model used, including the important variation in viscosity by over 12 orders of magnitude during vitrification. Next, the recently presented concept of the "set temperature" is reviewed; this temperature represents the transition from viscous to elastic dominance of straining that is associated with rapidly rising viscosity. It is shown in the current study that the effect of temperature gradients is fully captured with merely an elastic analysis, if the specimen is cooled to well below the set temperature. Elastic analysis is then applied to several cases, including close-form solutions for idealized shapes, and finite element analysis (FEA) for more complex geometries. From the close-form solutions, size limitations to avoid fractures, which depend on cooling rate, are identified. Finally, cooling to temperatures in the vicinity of the set temperature, which must account for both viscous and elastic responses, is studied numerically.

MATERIAL MODEL AND SOLUTION TECHNIQUES

The cryopreserved medium is assumed to have uniform and isotropic physical properties, with the only exception of the viscosity, which is the key property associated with vitrification. The viscosity of CPAs is largely unknown, but

limited data is available on DMSO, which is the key ingredient in many CPA cocktails. The viscosity of DMSO at various molar concentrations has been measured in the temperature range of 20°C to −45°C with falling ball viscometry;[15] the authors are unaware of viscosity measurements of DMSO at lower temperatures. While the physical properties of DMSO are concentration dependent, a reference concentration of 7.05 M DMSO has been selected in the current study. This concentration has been demonstrated to have similar physical properties to two CPA cocktails currently under investigation in parallel studies: DP6 (3 M DMSO, 3 M propylene glycol, and 2.4 g/l HEPES in EuroCollins solution) and VS55 (3.1 M DMSO, 2.2 M propylene glycol, 3.1 M formamide, and 2.4 g/l HEPES in EuroCollins solution).[12,16,17] Nevertheless, results presented in the current study are rather general, and the conclusions presented in the current study are not limited to a specific CPA and concentration.

The viscosity of DMSO in the temperature range of interest (in the vicinity of the glass transition temperature, T_g) is orders of magnitude higher than that in the range of available experimental data.[15] While T_g is commonly measured with differential calorimetry techniques (DSC), an alternative definition of glass transition is the temperature at which the viscosity reaches a value of 10^{12} Pa-s (10^{13} Poise). In the absence of viscosity data on cryoprotectants at low temperatures, the following functional behavior is assumed in the current study:[15]

$$\eta(T) = \eta_0 \exp\left(\frac{b}{T - T_0}\right) [Pa - s];$$

$$\eta_0 \equiv 10^{12} \exp\left(\frac{-b}{T_g - T_0}\right) \quad (1)$$

where η is the shear viscosity, and the parameters $b = 8.607$ K and $T_0 = 111.1$ K are selected to best fit the available experimental data on 7.05 M DMSO at higher temperatures,[12] and the glass transition temperature was taken to be −132°C, measured with DSC for 7.05 M DMSO.[16]

In uniaxial tension, the CPA is modeled with a simple viscoelastic law of the form:

$$\dot{\varepsilon} = \frac{1}{E}\frac{d\sigma}{dt} + \frac{\sigma}{3\eta} + \beta\frac{dT}{dt} \quad (2)$$

where $\dot{\varepsilon}$ is the strain rate, σ is the stress, E is the Young's modulus, and β is the coefficient of thermal expansion. This model describes the total strain rate as a linear superposition of [from left to right in Eq. (2)] the elastic strain rate, the viscous strain rate, and the thermal strain rate.[18] The uniaxial stress–strain behavior is generalized to multiaxial stresses assuming an isotropic response; the viscous strains are assumed to be incompressible, and the transverse elastic strains are based on a Poisson ratio ν. For all numerical solutions the following parameters were used: $E = 1$ GPa, $\nu = 0.2$, and $\beta = 2 \times 10^{-4}$ K^{-1}. The Poisson ratio, ν, would describe the behavior at low temperatures when viscous flow has ceased, and the CPA has solidified and become highly brittle; the value chosen is typical of glass and other brittle materials.[19] For simplicity, the variation in the thermal expansion β with temperature,[16,20] which was accounted for in earlier studies, is neglected here; $\beta = 2 \times 10^{-4}$ K^{-1} is a representative value at cryogenic temperatures. Preliminary data from experiments (unpublished) on the flow of DMSO near glass transition are consistent with the simple combination of linear elastic and Newtonian viscous behavior.

While the elastic solutions presented below for idealized geometries are based on exact closed-form solutions, solutions to more complex geometries and to viscoelastic problems were obtained using the general purpose finite element program, ANSYS 8.1. For axi-symmetric problems, elements of type Plane183 were used; for fully 3D problems, 20-noded SOLID186 brick elements were used. In calculations that account for the viscous deformation, special steps were taken to accommodate the variation in viscosity over many orders of magnitude within the simulated temperature range as discussed previously.[10,11]

TRANSITION FROM VISCOUS TO ELASTIC STRAIN REGIME

In a previous experimental study,[12] droplets of CPA were cooled on a very stiff substrate to low temperatures at which fractures occurred. Due to the higher thermal expansion of the CPA compared to the substrate, the CPA
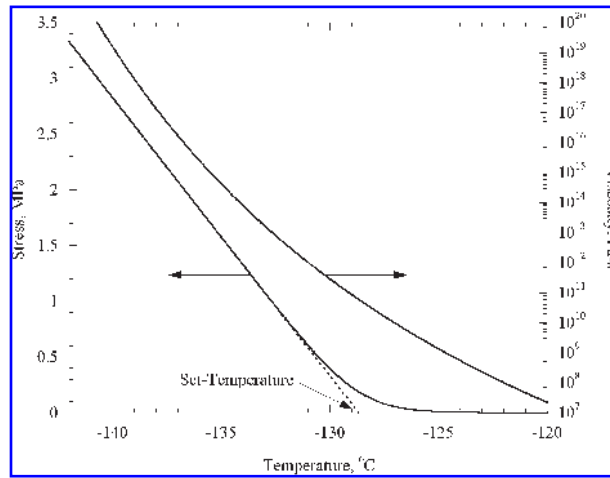
FIG. 1. Temperature-dependent viscosity used in the current study, and the resulting stress in a thin film of CPA.

droplet develops tensile stress. The droplet was modeled as a circular thin film; under this assumption, the stresses are equi-biaxial and uniform. The resulting stress in the CPA can be determined by integrating Equation (2), adapted for biaxial stress, using the viscosity as a function of temperature given in Equation (1). The resulting stress is presented in Figure 1, along with the viscosity as a function of temperature. It can be seen from Figure 1 that the stress in the droplet remains negligible at higher temperatures. Eventually, the stress increases and becomes linear with decreasing temperature, when the viscosity becomes sufficiently high. The set temperature is defined as the temperature obtained by back extrapolating from the linear portion of stress down to a zero stress value, as illustrated in Figure 1.

Based on the strain rate relationship presented in Equation (1), the set temperature can be estimated as the temperature at which the effects of viscous strain rate and elastic strain rate are similar in magnitude; this has been shown to take place when:[12]

$$P \equiv 3 \ \frac{d\eta}{dT} \ \frac{H}{E} \cong 1 \tag{3}$$

where H is the cooling rate. For a baseline case of $E = 1$ GPa and $H = 1°C/min$, one finds P equal to 0.988. Table 1 presents a comparison of set temperatures obtained in two ways: (1) by direct integration of Equation (2) for a thin film of CPA and back extrapolation, as illustrated in Figure 1, and (2) by using the estimate

presented in Equation (3), based on $P = 0.988$. Good agreement is found between the two methods of calculation. The set temperature is found to be a relatively weak function of E and H, due to the strong dependence of viscosity on temperature. Either way, given the viscosity function of Equation (1) and the associated parameters b and T_0, the set temperature is found to be within a relatively narrow range, at least over the range of cooling rates relevant to cryopreservation and for the plausible range of elasticity modulus for CPA.[12]

It has thus been established that the set temperature is a useful indicator of the relative contributions to deformation. Well above the set temperature, the elastic strain rate is insignificant, and the material behaves practically as a fluid. By contrast, well below the set temperature, the viscous strain is insignificant, and the material behaves practically as an elastic solid. This transition in behavior is critical to rationalizing two distinct responses to the temperature gradients induced by the cooling protocol.

The effect of cooling is captured in this study through a simple thermal history: a constant cooling rate on the specimen's outer surface, starting from a uniform initial temperature distribution, down to a prescribed storage temperature; the outer surface temperature remains constant thereafter. With temperature-independent properties, a quasi-steady distribution of temperature is reached during the period of cooling, with the temperature at all points decreasing at the same constant rate as the outer surface. If this steady distribution is achieved during sufficiently high temperatures, no stresses will exist in the material as it

TABLE 1. COMPARISON OF THE SET TEMPERATURE

Calculated by back extrapolation of the linear portion of stress with temperature for constrained thin film of cryoprotectant, $T_{set\ film}$ (see also Fig. 1), and approximated based on $p = 0.988$ in Eq. (3), $T_{set,P\ =\ 0.988}$.

H, °C/min	E, GPa	$T_{set\ film}$	$T_{set,\ P\ =\ 0.988}$
1	10	−130.6	−130.6
1	100	−132.3	−132.3
1	1000	−133.6	−133.8
10	1	−126.5	−126.6
100	1	−124.1	−124.1
1000	1	−121.1	−121.4

is cooled steadily to arbitrarily low temperatures, since the thermal strains are decreasing uniformly in space. Once the temperature at the outer surface reaches the storage temperature and is held constant, the temperature distribution in the domain gradually equilibrates toward a uniform final temperature distribution (the term "thermal equilibrium" is used in the text below in reference to a uniform temperature distribution in the domain, equal to the storage temperature). If this storage temperature is well below the set temperature, then upon approaching thermal equilibrium, the body will develop stresses that correspond to the thermoelastic problem of transitioning from the nonuniform, stress-free temperature distribution, associated with the constant cooling rate, to the final uniform temperature distribution. However, if the storage temperature is nearer to the set temperature, the deformations associated with temperature equilibration includes viscous and elastic strains occurring simultaneously, which must both be included in the analysis.

Figure 2 presents results of a representative process of cooling a bag of CPA well below the set temperature. While the specific parameters of the particular case are described in detail below (in the Numerical Solutions for Practical Shapes section), Figure 2 is discussed here in a qualitative manner only, for the purpose of identifying the effects of quasi-steady cooling (constant cooling rate) and equilibration of temperature. A cross-section of the CPA containing bag is illustrated in the inset of Figure 2, where the geometrical center point A and a point on the surface B are identified. As discussed above, stresses only begin to rise when cooling of the outer surface ceases and is held at constant temperature thereafter; these stresses are dictated by the elastic response of the material during the subsequent thermal equilibration.

ANALYSIS OF ELASTICITY BELOW THE SET TEMPERATURE

Analytical results for ideal shapes of an infinite plate, an infinite cylinder, and a solid sphere are presented in the next subsection.
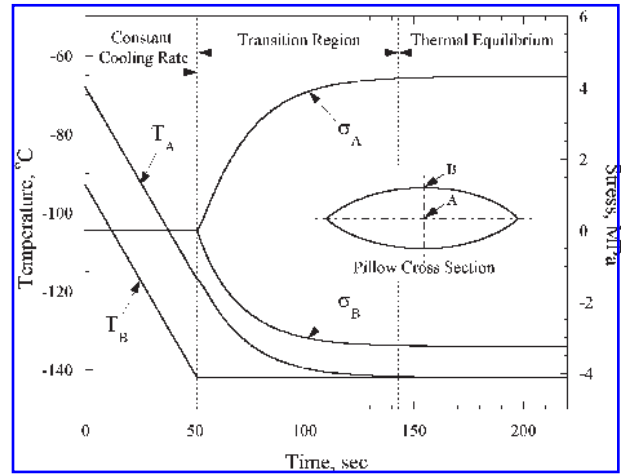

FIG. 2. Representative thermal and stress histories for cooling a pillow-like rectangular bag (Fig. 3) containing CPA; the inset schematically illustrates a cross-section of the bag, where A is the geometrical center point.

Numerical results for the more practical shapes of a finite cylinder (representing a vial of CPA) and two pillow-like shapes (representing a bag of CPA) are presented in the following subsection.

Analytic solutions for ideal shapes

For the ideal shapes, the temperature distribution during steady cooling and the stress distribution after thermal equilibration are dependent on a single coordinate. The temperature distribution is given by:

$$\frac{1}{\alpha} \frac{\partial T}{\partial t} = \frac{1}{x^n} \frac{\partial}{\partial x}\left(x^n \frac{\partial T}{\partial x}\right) \qquad (4)$$

where α is the thermal diffusivity ($k/\rho c_p$), t is the time and, x is the relevant coordinate, and n equals 0, 1, and 2 for the Cartesian, cylindrical, and spherical geometry, respectively. Equation (4) is subject to the boundary condition of:

$$T(\Omega) = \begin{cases} T_i - Ht & 0 < t < (T_i - T_s)/H \\ \\ T_s & (T_i - T_s)/H < t \end{cases} \qquad (5)$$

where Ω is the outer surface, T_s is the storage temperature, T_i is the initial temperature, and H is the cooling rate.

The solutions to the ideal shapes subject to zero normal and shear stresses at the boundary, are given by Boley and Weiner[21] for an ar-

bitrary function of temperature; in those solutions, the stresses are zero at an initial uniform temperature. In the current study, however, the initial stress distribution is zero, while the initial temperature distribution is nonuniform, corresponding to the quasi-steady temperature distribution resulting from Equations (4)–(5); stresses develop only as the temperature distribution equilibrates to the storage temperature, as described above. Hence, the final stress distributions are identical in magnitude, but negative in sign, to the stress distributions obtained by substituting the solutions to Equations (4)–(5) for the temperature distribution into the equations presented by Boley and Weiner.[21]

It can be seen from Equation (4) that if the cooling rate is constant, the temperature distribution is parabolically dependent on x, and the maximum temperature difference is dependent on d squared:

$$\Delta T = f \, \frac{Hd^2}{\alpha} \tag{6}$$

where the coefficient f is listed in Table 2. The characteristic length is the thickness for an infinite plate, and the diameter for a sphere and an infinite cylinder.

The order of magnitude of temperature differences that can be produced may be deduced as follows. The thermal conductivity, k, of 7.05 M DMSO at 273 K is 0.2 W/m-K,[22] while its value at very low temperatures is unknown; this value can impact the result substantially. Since DMSO is a water-based solution, and since the thermal conductivity of water increases exponentially with decreasing temperature,[23] a similar dependency might be assumed for DMSO.[10] Thus, the thermal conductivity of DMSO is assumed to be similar to that of ice, but shifted down to agree with the thermal conductivity value of DMSO at 273 K. It follows that the actual values for conductivity plausibly lies in the range of 0.2 W/m-K

and 6.5 W/m-K.[10] The density and specific heat are given representative values of 1100 kg/m³ and 2400 J/kg-K.[10] For the case of a cylinder, for example ($f = \frac{1}{16}$), a temperature difference of 25°C is produced for a vial diameter of 25 mm, cooling rate of 45°C/min, and thermal conductivity of 3 W/m-K; this case is studied below. Note that a much more substantial temperature difference would arise with the same cooling rate at higher temperatures, when the thermal conductivity is lower. While the underlying assumption that a steady-state temperature distribution is achieved might be questioned with such large temperature differences, the consequences of relaxing this assumption are left for future studies.

The maximum tensile stress corresponds to the in-plane stress for the plate, the axial stress for the cylinder, and the circumferential stress for the sphere; in all shapes, the stress is maximum at the geometric center of the domain. From the equations in ref. 21, the resulting maximum stresses for these ideal shapes can be presented in the form:

$$\sigma_{\max} = g \, \frac{E\beta\Delta T}{1 - \nu} \tag{7}$$

where the coefficient g is listed in Table 2 for various geometries.

*Numerical solutions for practical shapes*

To test its accuracy, FEA was applied to the prediction of the stresses in a plate and a sphere, subject to a constant cooling rate. This analysis predicted stresses that differed from the analytical result of Equation (7) by only 0.3% and 0.1%, respectively. With these reassuring results, FEA was applied to the pillow-like shapes illustrated in Figure 3, and to two cases of finite cylinders having length-to-diameter ratios of 9/5 (consistent with the vial used for prior studies[24]) and 1 (designated as the squat cylinder). Circular and rectangular pillow-like shapes were modeled as having maximum thickness 2h, with parabolic surfaces of the form:

$$z = \frac{h}{2}\left[1 - \left(\frac{r}{R}\right)^2\right] \tag{8}$$

$$z = \frac{h}{2}\left[1 - \left(\frac{x}{L_x}\right)^2\right]\left[1 - \left(\frac{y}{L_y}\right)^2\right] \tag{9}$$

TABLE 2. COEFFICIENTS FOR MAXIMUM TEMPERATURE DIFFERENCE AND MAXIMUM STRESS, EQS. (6), (7)

	Plate	Cylinder	Sphere
f	1/8	1/16	1/24
g	1/3	1/2	2/5
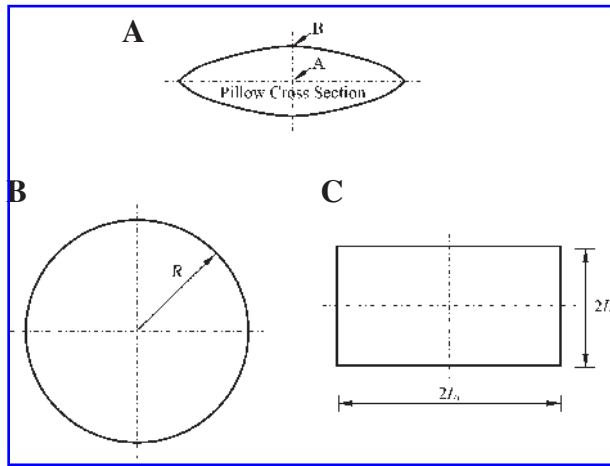
FIG. 3. Schematic illustration of pillow-like shapes analyzed by FEA: (**A**) Cross-section of the pillow, (**B**) top view of a circular pillow, Equation (8), and (**C**) top view of a rectangular pillow, Equation (9).

as illustrated in Figure 3. For heart valve cryopreservation, reasonable values of $2L_x = 122$ mm, $2L_y = 85$ mm, and $h = 13$ mm, were selected. Since the rectangular pillow-like bags are sealed in various ways to produce different ratios of L_y/L_x, and for purpose of simplicity in this study, only the square case of $2L_x = 122$ mm, $2L_y = 122$ mm, and $h = 13$ mm is considered. The circular pillow ($R = 61$ mm, and $h = 13$ mm) is given here for comparison purposes only, which has no direct application to cryopreservation.

The infinite cylinder solution overpredicts the maximum temperature difference in the vial by 3%, and the infinite flat plate solution overpredicts the maximum temperature difference in the rectangular pillow by 7%; the latter solution overpredicts the maximum temperature difference in the circular pillow by 1%. The maximum temperature difference in the squat

cylinder is between the predictions of an infinite cylinder and a sphere having the same radii. Comparisons for the maximum stress, normalized by $E\beta\Delta T/(1 - \nu)$, are listed in Table 3, where the temperature difference ΔT was taken from FEA. For the most part, maximum stresses from the idealized shapes serve as reasonable approximations for those found from the more realistic shapes. One exception is the pillow-like shapes, where the predicted stresses are up to 50% higher than the corresponding flat plate solution.

Critical characteristic length for fracture

It is commonly accepted that fracture is more likely to occur when the cooling rate is higher and the cryopreserved specimen is larger; this is consistent with the stress dependency exhibited in Equations (6)–(7). Quantitative estimates of the propensity for fracture can be obtained if the maximum tensile stress reached is compared with the critical stress for fracture σ_{crit}. Alternatively, the critical characteristic length, d_{crit}, above which the specimen is likely to fracture, can be calculated from:

$$d_{crit} = \sqrt{\frac{1 - \nu}{fg} \frac{\alpha}{\beta H} \frac{\sigma_{crit}}{E}} \qquad (10)$$

To gain insight into the critical characteristic length of the ideal shapes, Equation (10) was evaluated and the following material properties were applied. Based on experiments and analysis of the spontaneous fracture of a thin film of DMSO on a cooling substrate,[12] a critical stress of 3.2 MPa was assumed; this corresponded to an elastic modulus value of 1 GPa, to which the inferred critical stress is proportional.

TABLE 3. MAXIMUM STRESS NORMALIZED BY $E\beta\Delta T/(1 - \nu)$

Comparison of FEA predictions and analytical results by Eq. (7) for an infinite cylinder, σ_{ic}, sphere, σ_s, and an infinite plate, σ_{ip}. Axial stress is maximum for vial and squat cylinder; in-plane stress is maximum for the pillow-like shapes.

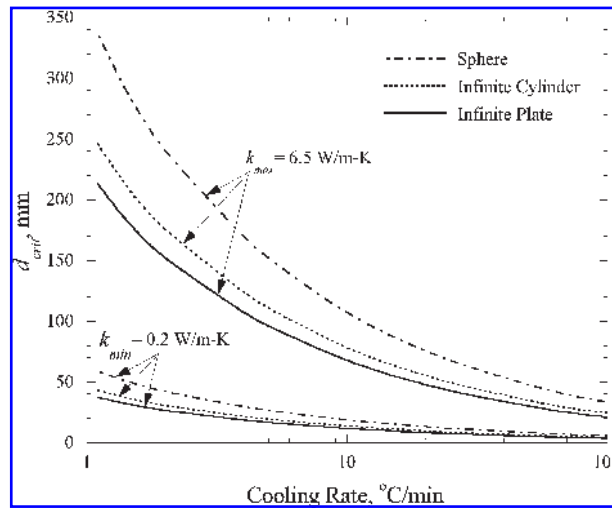| Configuration	FEA	Ideal shape approximation
Vial ($h/d_{ay} = 9/5$)	0.52	$\sigma_{ic} = 0.5$
Squat cylinder ($h/d_{ay} = 1$)	0.43	$\sigma_{ic} = 0.5, \sigma_s = 0.4$
Pillow (square)	0.48	$\sigma_{ip} = 0.33$
Pillow (circular)	0.45	$\sigma_{ip} = 0.33$

FIG. 4. Critical characteristic length as a function of the cooling rate for extreme values of thermal conductivity of 0.2 W/m-K and 6.5 W/m-K (corresponding to a critical stress level of 3.2 MPa, taken from Boley and Weiner[12]).

Figure 4 presents the critical characteristic length as a function of the cooling rate, for the ideal shapes, and for two extreme values of thermal conductivity, $k = 0.2$ W/m-K and 6.5 W/m-K. It can be seen from Figure 4 that the critical characteristic length is strongly dependent upon the thermal conductivity. For example, for a cooling rate of 20°C/min, the critical characteristic length varies by an order of magnitude from 10 mm to 100 mm. It can further be seen that a spherical shape generates the lowest stress, and that an infinite plate generates the highest stress, out of the three cases under consideration; thus, the former permits a greater critical size then the latter. However the thermal conductivity effect overwhelms the shape effect, in the range of properties studied here. For each set of conditions, the critical characteristic length is inversely proportional to the square root of the cooling rate, Equation (8).

STRESSES UPON COOLING TO INTERMEDIATE TEMPERATURES

The discussion now turns to the effect of the storage temperature on stress. Thus far, the specimen was presumed to be cooled at a constant cooling rate to well below the set temperature, where the viscosity is effectively in-finite. If cooling of the specimen is to be halted at higher temperatures, in the vicinity of the set temperature, the resulting stresses would be lower.

Figure 5 presents results for a finite cylinder representing a vial, with a 25°C temperature difference between the outer surface and the center during steady cooling. The axial stress σ_z is plotted in Figure 5 for several radial locations across the central plane of the vial as a function of the storage temperature; this is the stress reached when the distribution throughout the volume has effectively equilibrated to the storage temperature. (After a very long period of time, the stresses would relax to zero if storage temperature were not sufficiently low.) Notice that no stress develops if the storage temperature is too high. In addition, all stresses approach asymptotically the values corresponding to fully elastic stress development (addressed in the previous section) if the storage temperature is sufficiently low.

Note that stresses begin to rise only when the storage temperature reaches −127.0°C. For the cooling rate that produces a 25°C difference in the vial ($H = 45$°C/min), and for an elastic modulus of 1 GPa, the set temperature was determined from Equation (3) to be −125.0°C.
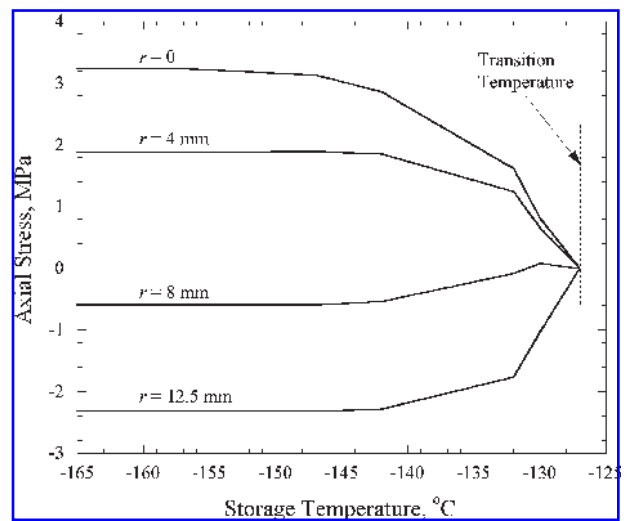

FIG. 5. Axial stress at the mid-height of a finite cylinder after it reaches thermal equilibrium, as a function of the storage temperature. The various curves represent the stress at several radial locations, where the cylinder height is 45 mm, its diameter is 25 mm, the cooling rate is 45°C/min, and the maximum temperature difference across the cylinder is 25°C.
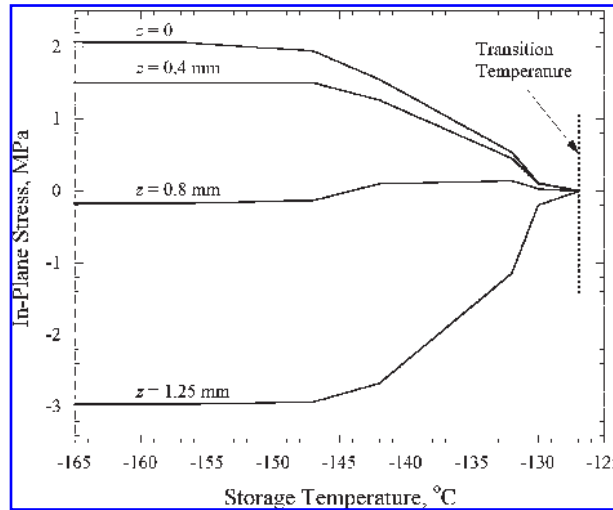
FIG. 6. In-plane stress in an infinite plate after it reaches thermal equilibrium, as a function of the storage temperature. The various curves represent the stress at several distances from the plate centerline, where the plate thickness is 2.5 mm, the cooling rate is 50°C/min, and the maximum temperature difference across the plate is 25°C.

Thus, the set temperature determined for a thin film on a substrate[12] has relevance to the current, quite distinct but technologically important, problem of stress development due to temperature gradients in a vial. Note that the center point in the domain has the highest tensile stress regardless of the final temperature. The same behavior is observed for the cases of the plate and the sphere (Figs. 6 and 7). Using the appropriate cooling rates of 50°C/min and 66°C/min, the set temperature is determined to be −124.9°C and −124.6°C for the plate and sphere, respectively; therefore, it is not surprising that the stress tends to rise from zero at approximately the same temperature of −127°C. For the purpose of a more detailed analysis, a "transition temperature" is defined in the current study as the storage temperature at which the stress first begins to rise noticeably upon thermal equilibration. While the transition temperature cannot be quantified precisely, it approximately equals −127°C in the current case, which is a few degrees below the set temperature. One could expect the stresses to depend on the temperature difference between the storage temperature and the transition temperature, as well as on the maximum temperature difference within the body during constant cooling.

To allow one to approximate stress for intermediate storage temperatures, while avoiding the need to repeatedly perform full scale viscoelastic calculations, which are computationally expensive, results are replotted in Figure 8 as normalized stress versus dimensionless storage temperature. Here, the stress is normalized by its elastic value, corresponding to the same geometry and same temperature difference between inside and outside. The dimensionless storage temperature is defined as:

$$\theta = \frac{T_{\text{trans}} - T_{\text{storage}}}{\Delta T} \quad (12)$$

where T_{trans} is the transition temperature, T_{storage} is the storage temperature, and ΔT is the maximum temperature difference during steady cooling. The dimensionless storage temperature indicates the extent to which the body is cooled below transition, relative to the temperature difference between the outside and inside during steady cooling. At $\theta = 1$, the center point of the domain (the point for which stresses are presented) reaches transition just as the steady cooling ceases. The maximum temperature difference during constant cooling is 25°C for all the cases shown in Figure 8. While the curves for the different cases presented in Figure 8 differ in details, they display
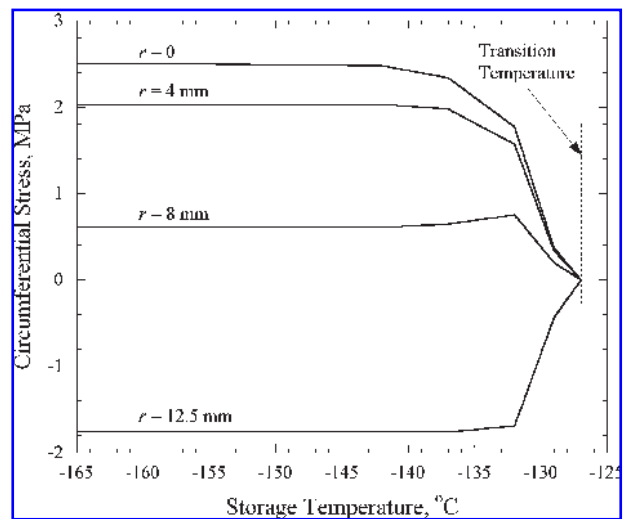

FIG. 7. Circumferential stress in a sphere after it reaches thermal equilibrium as a function of the storage temperature. The various curves represent stress at several radial locations, where the sphere diameter is 25 mm, the cooling rate is 66°C/min, and the maximum temperature difference is 25°C.
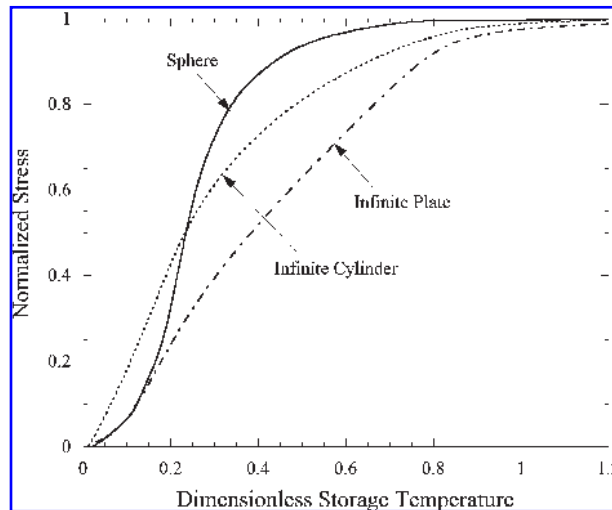
FIG. 8. Maximum normalized stress as a function of dimensionless storage temperature, Equation (12), for ideal shapes.

a similar general trend, that the stress exceeds 90% of its elastic value before $\theta = 1$.

Based on the current observations, a method of approximating the maximum stress, for other parameter values and viscosity functions of temperature, is proposed as follows. First, elastic calculations (requiring no viscoelastic analysis) are to be performed for the geometry in question. These calculations may be performed for a single cooling rate, since the stresses are linearly proportional to the cooling rate, provided that there is sufficient time for a quasi-steady temperature distribution to develop. (One may further choose to use one of the idealized shapes presented above.) Next, the set temperature is determined, either through integration of Equation (2), or through the approximation discovered above, namely $P = 0.988$; either way, the appropriate viscosity function of temperature must be used. Based on the current results for DMSO, the transition temperature at which the stresses first start rising is estimated as 2°C below the set temperature. Finally, the normalized stress as a function of the dimensionless temperature presented in Figure 8 is used to estimate the specific maximum stress developed in the specimen.

To validate the new method of approximating the maximum stress, several additional cases for the vial shape were studied. As dis-

cussed above, the thermal conductivity at low temperatures is associated with a significant level of uncertainty, which may have an impact on the calculated stress, where the temperature gradient increases with decreasing thermal conductivity. (The specific heat is assumed constant in the current case; therefore, the thermal conductivity is proportional to the thermal diffusivity). Here, calculations were carried out for cooling to a specific storage temperature of −132°C, for various cooling rates and thermal conductivity values. In all cases, the set temperature was recomputed (for the given cooling rate), and the transition temperature was set to be 2°C below the set temperature. The temperature difference is distinct for each set of parameters; this difference determines the elastic stress and, hence, the normalization of the stress and the storage temperature. It can be seen in Figure 9 that for all studied cases, the new results agree very well with the baseline curve of normalized stress versus dimensionless storage temperature ($H = 45°C/min$ and $k = 3$ W/m-K). These results validate the proposed simplified method of maximum stress approximation.

As a second validation test for the method, the effect of a different CPA, DP6, was ana-
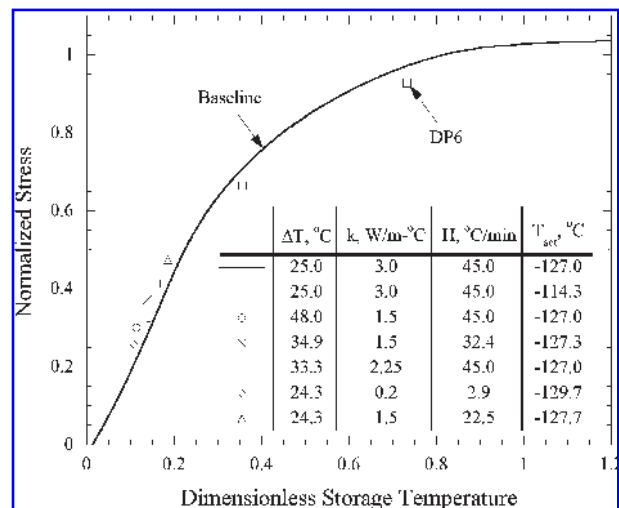

FIG. 9. Comparison of normalized stress as a function of the dimensionless storage temperature, Equation (12), subject to various thermal parameters; all results correspond to a cylinder having a length of 45 mm and a diameter of 25 mm, representative of a vial in previous studies.[10] Except for the three data points identified for the CPA cocktail DP6, all other data points refer to DMSO properties.

lyzed. The temperature-dependence of the viscosity of DP6 was fit to Equation (1) in a previous study,[12] with $b = 5.45$ K and $T_0 = 132.3$ K. The set temperature was found by integration to be $-116.3°C$, for the baseline case of $E = 1$ GPa and $H = 1°C/min$; the ratio of P was found to be 0.990, nearly the same value as for DMSO. Using the viscosity function of temperature for DP6, stresses were determined by means of FEA for the vial shape, when cooled to three different storage temperatures, and subject to the same temperature difference of $25°C$ ($H = 45°C/min$ and $k = 3$ W/m-K). The normalizing elastic stresses are the same for DP6 as they were for DMSO, and are independent of the viscosity. The dimensionless storage temperature requires the transition temperature, which is estimated as $2°C$ below the set temperature, following the procedure described above. The set temperature for DP6 in this case, was found to be $-113.4°C$, using the fixed value of the ratio P. Therefore, the transition temperature was presumed to be $-115.4°C$. The dimensionless storage temperature corresponding to the three different storage temperatures, as well as the stresses, are also presented in Figure 9. It can be seen from Figure 9 that good agreement is found between the new data points and the previously drawn curve for DMSO, further supporting the generality of the newly proposed method.

SUMMARY AND CONCLUSIONS

To gain insight into the propensity for cracking to occur during cryopreservation via vitrification, stresses which develop in a mass of cryoprotectant, subject to a constant cooling rate down to a preset storage temperature, have been studied. The temperature-dependent viscosity is shown to play a critical role in the development of stresses. In particular, the recently defined set temperature, which depends primarily on the temperature dependency of viscosity, separates the storage temperature into stress development regimes. Negligible stresses arise when the storage temperature is above the set temperature, while far below the set temperature, stresses approach levels that are independent of the viscosity and can be determined by merely an elastic analysis. At temperatures slightly below the set temperature, analysis accounting for both viscous and elastic straining is necessary.

For storage temperatures far below the set temperature, the stresses have been found to be proportional to the cooling rate, the elastic modulus, the characteristic dimension of the domain to the second power, and the thermal expansion coefficient; these stresses are inversely proportional to the thermal conductivity. Analytic expressions for the stress have been found for simple shapes, which are demonstrated to be credible approximations for stresses in more complex shapes, where the latter can only be found from computationally expensive FEA. FEA simulations accounting for viscoelastic material behavior were used to determine stresses when the storage temperature is not well below the set temperature. A normalization of stress and storage temperature approximately condenses the predicted stresses, as shown for a number of different geometries and cooling conditions, enabling one to estimate stresses for the entire range of storage temperatures, without resorting to viscoelastic analysis. Stresses are found to approach those based on elastic modeling, provided that the location of highest temperature (usually at the center of the domain) exceeds the set temperature during the period of steady cooling.

This work has indicated the importance of measuring the key properties of CPAs, such as viscosity and thermal conductivity, in the cryogenic temperature range. The current study suggests potential strategies for simplified calculations of mechanical stresses, with the goal of establishing tools for efficient optimization of cryopreservation. Specifically, it is demonstrated that one could produce very low stresses by cooling down very rapidly to just above the set temperature and allowing thermal equilibration to occur; further cooling could then be accomplished much more slowly to the final temperature. Experiments to test this prediction are also underway.

REFERENCES

1. Lin S, Gao DY, Yu XC. Thermal stress induced by water solidification in a cylindrical tube. ASME J Heat Trans 1990;112:1079–1082.
2. Rubinsky B, Cravalho EG, Mikic B. Thermal stress in frozen organs. Cryobiology 1980;17:66–73.
3. Gao DY, Lin S, Watson PF, et al. Fracture phenomena in an isotonic salt solution during freezing and their elimination using glycerol. Cryobiology 1995;32:270–284.
4. Rabin Y, Steif PS. Thermal stress modeling in cryosurgery. Int J Solids Struct 2000;37:2363–2375.
5. Rabin Y, Steif PS. Analysis of thermo-mechanical stress in cryopreservation. CryoLetters 2005;26:409–411.
6. Taylor MJ, Song YC, Brockbank KGM. Vitrification in tissue preservation: New developments. In: Fuller BJ, Lane N, Benson EE, eds. *Life in the Frozen State.* New York: CRC Press; 2004:603–641.
7. Fahy GM, MacFarlane DR, Angell CA, et al. Vitrification as an approach to cryopreservation. Cryobiology 1984;21:407–426.
8. Pegg DE, Wusteman MC, Boylan S. Fractures in cryopreserved elastic arteries. Cryobiology 1997;34:183–192.
9. Steif PS, Palastro M, Wen CR, et al. Cryomacroscopy of vitrification, Part II: Experimental observations and analysis of fracture formation in vitrified VS55 and DP6. Cell Preservat Technol 2005;3:184–200. Website in conjunction with this paper: *http://www.me.cmu.edu/faculty1/rabin/CryomacroscopyImages01.htm*
10. Steif PS, Palastro MC, Rabin Y. Continuum mechanics analysis of fracture progression in the vitrified cryoprotective agent DP6. ASME Biomech Eng, 2007.
11. Steif PS, Palastro MC, Rabin Y. Analysis of the effect of partial vitrification on stress development in cryopreserved blood vessels. Med Eng Phys 2007;29:637–728.
12. Rabin Y, Steif PS, Hess KC, et al. Fracture formation in vitrified thin films of cryoprotectants: Cryobiology 2006;53:75–95. Website in conjunction with this paper: *http://www.me.cmu.edu/faculty1/rabin/CryomacroscopyImages02.htm*
13. Luyet BJ. The vitrification of organic colloids and of protoplasm. Biodynamica 1937;1:1–14.
14. Song YC, Khirabadi BS, Lightfoot FG, et al. Vitreous cryopreservation maintains the function of vascular grafts. Nat Biotechnol 2000;18:296–299.
15. Schichman SA, Amey RL. Viscosity and local liquid structure in dimethyl sulfoxide–water mixtures. J Phys Chem 1971;75:98–102.
16. Plitz J, Rabin Y, Walsh JR. The effect of thermal expansion of ingredients on the cocktails VS55 and DP6. Cell Preservat Technol 2004;2:215–226.
17. Rabin Y, Plitz J. Thermal expansion of blood vessels and muscle specimens permeated with DMSO, DP6, and VS55 in cryogenic temperatures. Ann Biomed Eng 2005;33:1213–1228.
18. Malvern LE. *Introduction to the Mechanics of a Continuous Medium.* Englewood Cliffs, NJ: Prentice-Hall; 1969.
19. Richerson DW. Modern ceramic engineering: Properties, processing, and use in design. New York: Marcel Dekker, Inc.; 1992.
20. Jimenez Rios JL, Rabin Y. Thermal expansion of blood vessels in low cryogenic temperatures. Part II: Measurements of blood vessels vitrified with VS55, DP6, and 7.05M DMSO. Cryobiology 2006;52:284–294.
21. Boley BA, Weiner JH. *Theory of Thermal Stresses.* New York: Wiley; 1960.
22. Nieto-Draghi C, Avalos JB. Transport properties of dimethyl sulfoxide aqueous solutions. J Chem Phys 2003;119:4782–4789.
23. Rabin Y. The effect of temperature-dependent thermophysical properties in heat transfer simulations of biomaterials in cryogenic temperatures. CryoLetters 2000;21:163–170.
24. Rabin Y, Taylor MJ, Walsh JR, et al. Cryomacroscopy of vitrification, Part I: A prototype and experimental observations on the cocktails VS55 and DP6. Cell Preserv Technol 2005;3:169–183. Website in conjunction with this paper: http://www.me.cmu.edu/faculty1/rabin/CryomacroscopyImages01.htm

Address reprint requests to:
Yoed Rabin
Biothermal Technology Laboratory
Department of Mechanical Engineering
Carnegie Mellon University
500 Forbes Avenue
Pittsburgh, PA 15237

E-mail: Rabin@CMU.EDU